catalysts

MDPI

Article

Mechanism of Guaiacol Hydrodeoxygenation on Cu (111): Insights from Density Functional Theory Studies

Destiny Konadu [1], Caroline Rosemyya Kwawu [1,*], Richard Tia [1], Evans Adei [1] and Nora Henriette de Leeuw [2,3]

[1] Department of Chemistry, Kwame Nkrumah University of Science and Technology, Kumasi 1916, Ghana; dkonadu1@st.knust.edu.gh (D.K.); richardtia.cos@knust.edu.gh (R.T.); eadei.sci@knust.edu.gh (E.A.)
[2] Department of Chemistry, Cardiff University, Cardiff CF1 3AT, UK; deleeuwn@cardiff.ac.uk
[3] School of Chemistry, University of Leeds, Cardiff CF1 3AT, UK
* Correspondence: kwawucaroline@knust.edu.gh

Abstract: Understanding the mechanism of the catalytic upgrade of bio-oils via the process of hydrodeoxygenation (HDO) is desirable to produce targeted oxygen-deficient bio-fuels. We have used calculations based on the density functional theory to investigate the reaction mechanism of HDO of guaiacol over Cu (111) surface in the presence of H_2, leading to the formation of catechol and anisole. Our analysis of the thermodynamics and kinetics involved in the reaction process shows that catechol is produced via direct demethylation, followed by dehydrogenation of –OH and re-hydrogenation of catecholate in a concerted fashion. The de-methylation step is found to be the rate-limiting step for catechol production with a barrier of 1.97 eV. Formation of anisole will also proceed via the direct dehydroxylation of guaiacol followed by hydrogenation. Here, the rate-limiting step is the dehydroxylation step with an energy barrier of 2.07 eV. Thermodynamically, catechol formation is favored while anisole formation is not favored due to the weaker interaction seen between anisole and the Cu (111) surface, where the binding energies of guaiacol, catechol, and anisole are -1.90 eV, −2.18 eV, and −0.72 eV, respectively. The stepwise barriers also show that the Cu (111) surface favors catechol formation over anisole as the rate-limiting barrier is higher for anisole production. For catechol, the overall reaction is downhill, implying that this reaction path is thermodynamically and kinetically preferred and that anisole, if formed, will more easily transform.

Keywords: guaiacol; copper; hydrodeoxygenation; biomass; lignin; DFT

Citation: Konadu, D.; Kwawu, C.R.; Tia, R.; Adei, E.; de Leeuw, N.H. Mechanism of Guaiacol Hydrodeoxygenation on Cu (111): Insights from Density Functional Theory Studies. *Catalysts* **2021**, *11*, 523. https://doi.org/10.3390/catal11040523

Academic Editor: Emmanuel M. Papamichael

Received: 22 March 2021
Accepted: 6 April 2021
Published: 20 April 2021

1. Introduction

Lignocellulosic biomass is a promising renewable carbon carrier that could reduce our over-dependence on fossil fuels. Lignin is the second largest constituent of lignocellulosic biomass, where it accounts for approximately 25% of the biomass [1] and consists of cross-linked phenolic polymers [2]. Bio-oils obtained from fast pyrolysis of lignin have high oxygen contents, usually more than 10 wt% and sometimes as much as 50 wt% [3]. Thus, depolymerized products obtained after fast pyrolysis are subjected to a catalytic process for oxygen removal. Hydrodeoxygenation (HDO) is considered a critical reaction in the oxygen removal from pyrolyzed lignin, leading to hydrocarbon fuels and high value-added chemicals (such as benzene, toluene, and other aromatics) [4,5]. HDO reactions are typically performed in the presence of a solid-phase catalyst, a liquid-phase phenol substrate, and gas-phase molecular hydrogen (H_2) and usually occur at relatively high temperatures of 300–500 °C [6]. Solid-phase catalysts used for bio-oil upgrading should not only improve the selectivity towards desired products, but should also provide an alternative lower energy pathway in the depolymerization reaction [7]. Noble metals exhibit better deoxygenation performance compared to sulfide-based catalysts [8], but their cost is considerable and cheaper metal alternatives like Fe, Cu, or Ni are being explored.

Several reaction pathways have been proposed for HDO and the reactions that accompany HDO [9]. Understanding of these reaction pathways have led to studies focused

on investigations of various individual model compounds over different catalysts, due to the complexity of the bulk lignin polymer [10]. Several pathways have been proposed for the removal of oxygen with H_2 using model compounds such as guaiacol, a compound that a number of researchers have considered to be a prototype [3]. Guaiacol, $C_6H_4(OH)(OCH_3)$, is a lignin building block bearing two oxygen-containing functional groups (–OH and $–OCH_3$) with structural similarity to coniferyl alcohol, which is a major constituent of lignin [11].

The preferred reaction pathway to individual products depends substantially on the type of catalyst used [12]. In an attempt to enhance the performance of the HDO reaction, intensive efforts have been devoted to designing solid-phase catalysts with high efficiency for the cleavage of the C_{aryl}–OH bond, which features a high dissociation enthalpy (465 kJ mol^{-1}) [13,14]. An approximate idea of the mechanism for the HDO of aromatics on various (metallic and non-metallic) catalysts can be gained from a large number of experiments, including isotope labeling and the analysis of intermediate species, as well as products observed under processing conditions [15–22]. For example, guaiacol HDO on Pt/Al_2O_3 has been suggested to proceed via the intermediates catechol and phenol [12], but the atomic-level processes occurring at the catalyst surface remain unclear. Other reactions involving aromatics, e.g., their dehydrogenation [23–26] or the conversion of benzene to phenol, have been explored computationally for surfaces of Rh, Ni, Pd, Pt, and Cu. The adsorption of aromatic oxygenates, such as phenol, anisole, cresol, or the more complex 1,3,5-trihydroxybenzene, have been the subject of computational studies on pure Rh [25], Ni [27], Pd [3], and Pt [25,28–30] surfaces, as well as on surfaces of alloys such as FePd [3] or CuNi [30].

Although various computational works have addressed the HDO of aromatics over metallic [6,12,18,31,32] and non-metallic [33] catalysts, in many cases the studies are limited to the adsorption of various model substrates on the catalyst surface [32,33]. However, a computational exploration of the reaction network is still missing, with the exception of Ru and Pt [15,34]. Hence, this study explores the detailed mechanism of HDO on the Cu (111) surface to understand the reaction pathway leading to desired HDO products, such as catechol and anisole, with the aim of identifying an efficient copper surface for the upgrade of bio-oil into hydrocarbon fuels.

2. Computational Details

As applied in the Quantum ESPRESSO package [35], the density functional theory (DFT) technique was used during all calculations. The plane-wave basis sets, as well as the ultra-soft pseudopotentials, were used within the generalized gradient approximation. This performs fully self-consistent DFT calculations to solve the Kohn-Sham equations [35]. The Perdew Burke Ernzerhof (PBE) GGA exchange-correlation functional was employed [36] and the Fermi-surface effects were treated by the smearing technique of Fermi-Dirac, using a smearing parameter of 0.003 Ry. An energy convergence threshold defining self-consistency of the electron density was set to 10^{-6} eV and a beta defining mixing factor for self-consistency of 0.2. The Grimme's D2 correction was implemented for dispersion corrections. The graphics of the atomic structures and the iso-surfaces of the differential electron density plots have been prepared with the XCrysDen software [37].

For all surface descriptions, the slab models were employed. Periodic boundary conditions are applied such that the central super-cell is reproduced periodically throughout space [38]. A vacuum region, of 20 Å, was introduced to all surfaces to avoid interactions between slabs. Energy cut-offs of 40 Ry (544 eV) were considered for all systems with a corresponding charge density cut-off of 320 Ry (4354 eV). A Monkhorst-Pack k-point grid of ($7 \times 7 \times 7$) and ($1 \times 1 \times 1$) were sampled in the Brillioun zones of the bulk and p (4×4) surface slab, respectively [39]. Transition states were searched using the climbing image nudged elastic band (CI-NEB) method implemented in Quantum-Espresso. The CI-NEB was implemented by interpolating three images between the initial and final states and optimizing the images along the reaction coordinate. Each transition state was confirmed

to have a single imaginary vibrational frequency. A p (4 × 4) supercell of copper was employed in all calculations, comprising 64 copper atoms. The top three Cu layers of each slab were relaxed while the Cu atoms in the bottom layers were kept fixed at the optimized bulk positions to mimic the bulk. All gas-phase molecules were optimized in a 10 × 10 × 10–unit cell. We denote all the adsorbates under study by labels **1** to **13** (see Figure 1). Labels of type **1–2** denote the transformation from adsorbate **1** to adsorbate **2.**

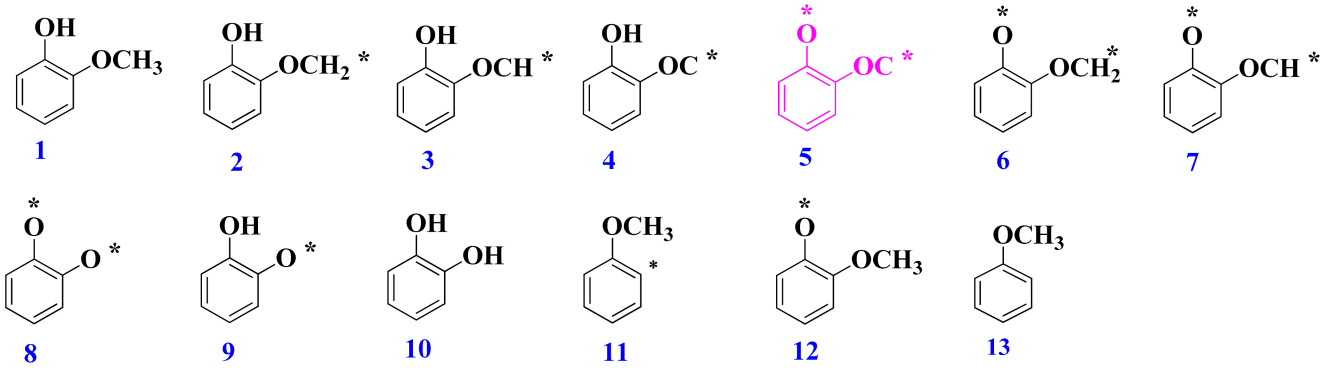

Figure 1. Structures of compounds (reactant, intermediates, and products) under study. An asterisk indicates bound (di-)radical site(s) to the metal surface. Structure 5 is not a stable structure on the surface, as it disintegrates.

The reaction energy was calculated as:

$$\Delta E_{rxn} = E_{(p)} - E_{(r)} \quad (1)$$

where $E_{(p)}$ is the energy of the intermediate formed and $E_{(r)}$ is the energy of the reactants.

The relative activation barrier was obtained by using the equation:

$$\Delta E_a = E_{(ts)} - E_{(IS)} \quad (2)$$

where $E_{(ts)}$ is the energy of the transition state and $E_{(IS)}$ is the energy of the intermediate from which the transition state is formed.

The structures of reactant, products, and intermediates involved in the reaction network are shown in Figure 1, while a pictorial view of the substrate-adsorbate bound states is shown in Figure 2. The stepwise reaction scheme for the conversion of guaiacol was considered via four pathways (see Figure 3).

As shown in Figure 3, four different reaction pathways and their stepwise elementary steps have been investigated in the reaction network and the sequence of the reactions can be deduced as follows; Pathway A (dehydrogenation path) involves the initial removal of hydrogen from the alkyl group and the possible transformations thereafter by hydrogenation to structure **10** i.e., catechol. Pathway B (demethylation path) involves the initial direct removal of $–CH_3$ and transformation into catechol. Pathway C (dehydrogenation) involves the initial dehydrogenation of the hydroxyl group to produce both structures **13** and **10,** i.e., anisole and catechol. Finally, pathway D (dehydroxylation) entails the direct dehydroxylation to form anisole. Transition state structures of all elementary steps and their respective imaginary frequencies are shown in Figure 4 and Table 1, respectively. These elementary steps explored pathways A, B, C, and D are based on proposed pathways for the formation of HDO compounds [34,40].

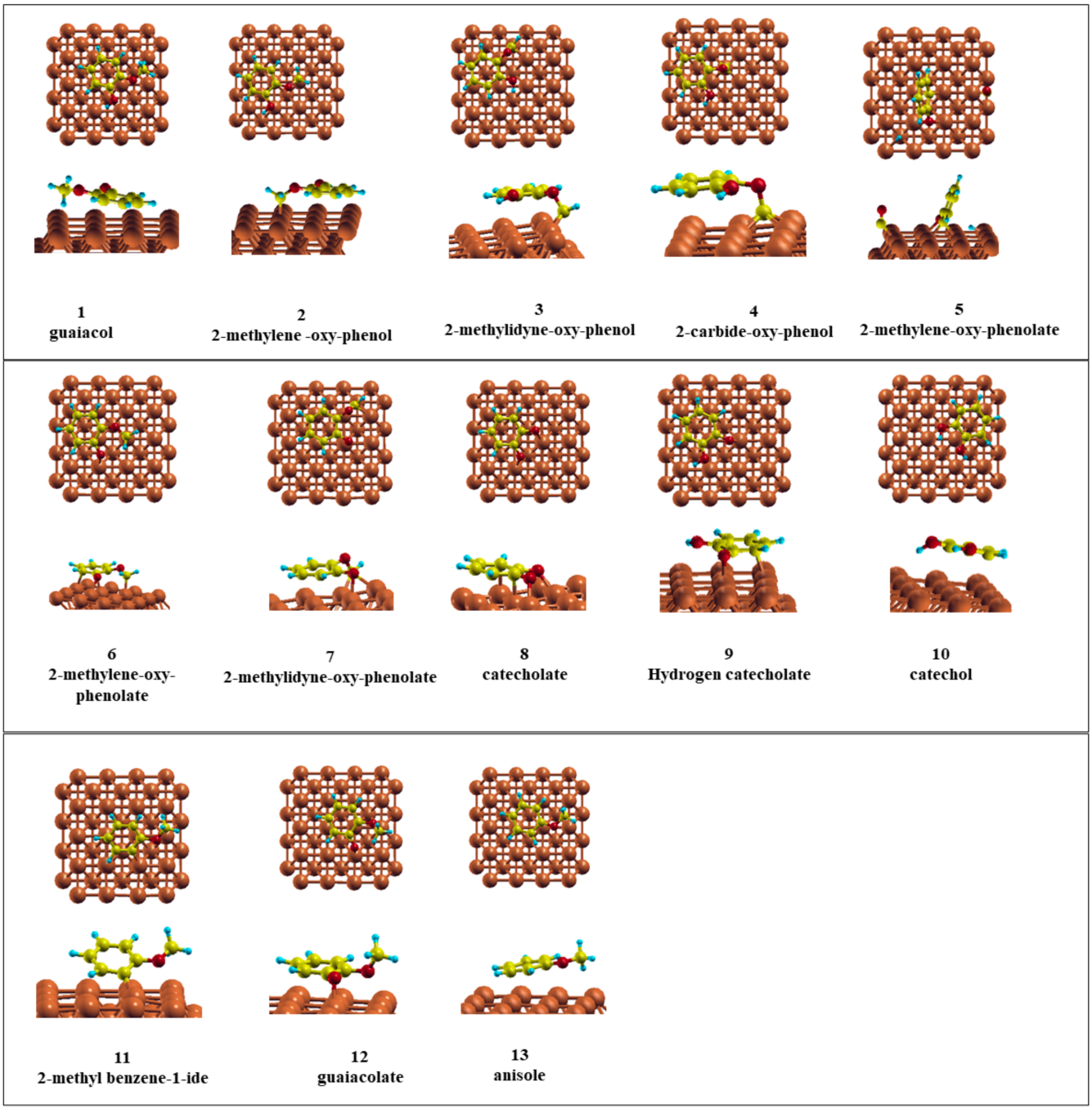

Figure 2. Optimized structures of adsorption complexes viewed from the top and the side. Cu: brown; O: red; C: yellow; H: blue. Structure 5 is not a stable structure on the surface, as it disintegrates.

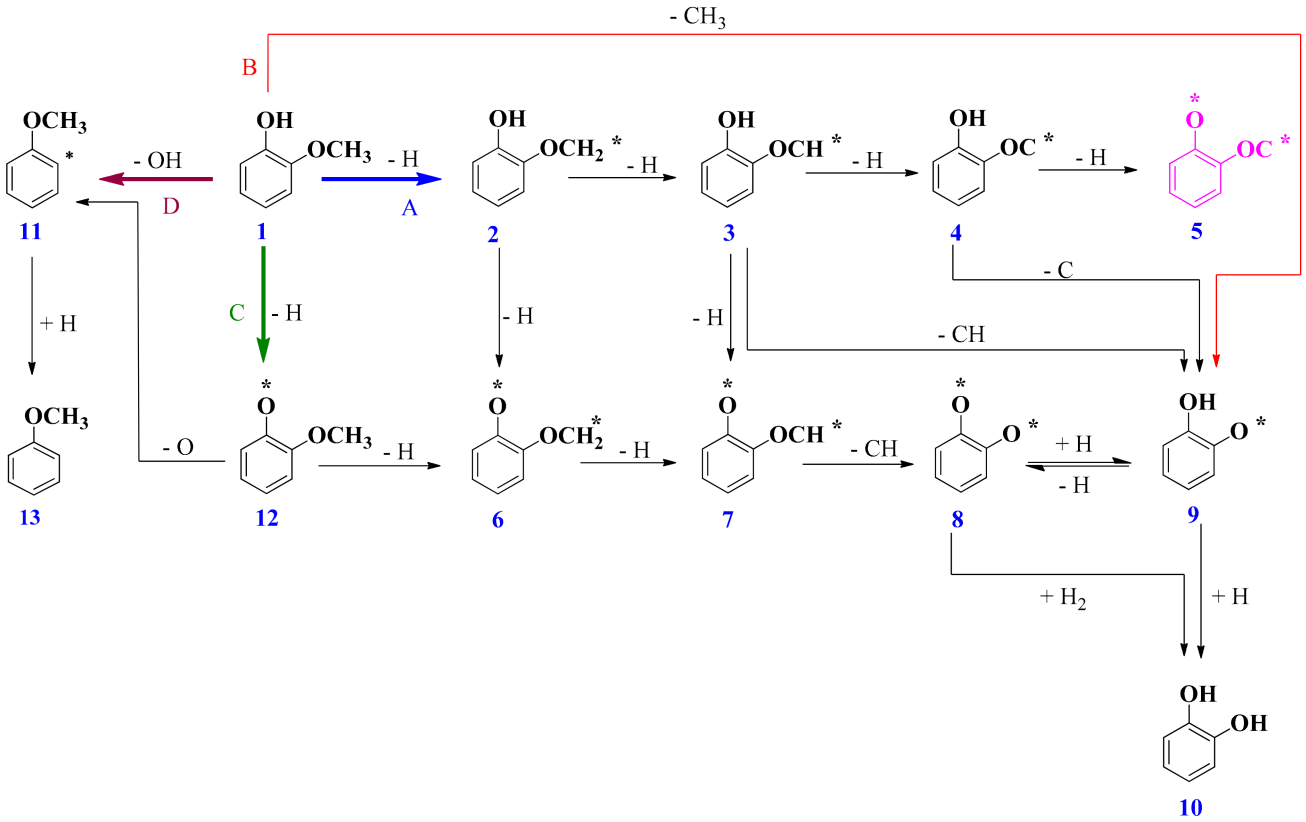

Figure 3. The four reaction paths (A, B, C, and D) and networks considered for the conversion of guaiacol to catechol and anisole. * indicates on the adsorbate, the sites of decomposition and radical formation.

Table 1. Chemical equations for the elementary reaction steps involved in the HDO reaction of guaiacol, the transition state structures, and the single imaginary frequencies for the transition states on Cu (111).

Reaction	E_{rxn}/eV	E_a/eV	TS
$C_6H_4(OH)(OCH_2) \rightarrow C_6H_4(OH)(OCH) + H$	−0.22	2.16	TS 2–3
$C_6H_4(OH)(OCH) \rightarrow C_6H_4(O)(OCH) + H$	0.74	3.34	TS 3–7
$C_6H_4(O)(OCH_3) \rightarrow C_6H_4(O)(OCH_2) + H$	−0.75	1.98	TS 12–6
$C_6H_4(O)(OCH_2) \rightarrow C_6H_4(O)(OCH) + H$	0.74	4.39	TS 6–7
$C_6H_4(O)(OCH) \rightarrow C_6H4(O)(O) + CH$	−1.43	0.33	TS 7–8
$C_6H_4(OH)(OCH) \rightarrow C_6H_4(OH)(O) + CH$	−1.66	3.03	TS 3–9
$C_6H_4(OH)(OCH) \rightarrow C_6H_4(OH)(OC) + H$	0.57	0.64	TS 3–4
$C_6H_4(OH)(OC) \rightarrow C_6H_4(OH)(O) + C$	−1.70	1.39	TS 4–9
$C_6H_4(O)(O) + H \rightarrow C_6H_4(O)(OH)$	−1.66	0.17	TS 8–9
$C_6H_4(O)(OH) + H \rightarrow C_6H_4(OH)(OH)$	−2.03	5.17	TS 9–10
$C_6H_4(O)(O) + H_2 \rightarrow C_6H_4(OH)(OH)$	−2.03	0.22	TS 8–10
$C_6H_4(OH)(OCH_2) \rightarrow C_6H_4(O)(OCH_2) + H$	−0.75	0.60	TS 2–6
$C_6H_4(OCH_3) + H \rightarrow C_6H_5(OCH_3)$	0.41	1.25	TS 11–13
$C_6H_4(O)(OCH_3) \rightarrow C_6H_4(OCH_3) + O$	−0.61	2.65	TS 12–11
$C_6H_4(OH)(OCH_3) \rightarrow C_6H_4(OH)(OCH_2) + H$	−0.78	3.50	TS 1–2
$C_6H_4(OH)(OCH_3) \rightarrow C_6H_4(OH)(O) + CH_3$	−1.70	1.97	TS 1–9
$C_6H_4(OH)(OCH_3) \rightarrow C_6H_4(O)(OCH_3) + H$	−1.50	0.99	TS 1–12
$C_6H_4(OH)(OCH_3) \rightarrow C_6H_4(OCH_3) + OH$	−0.61	2.07	TS 1–11

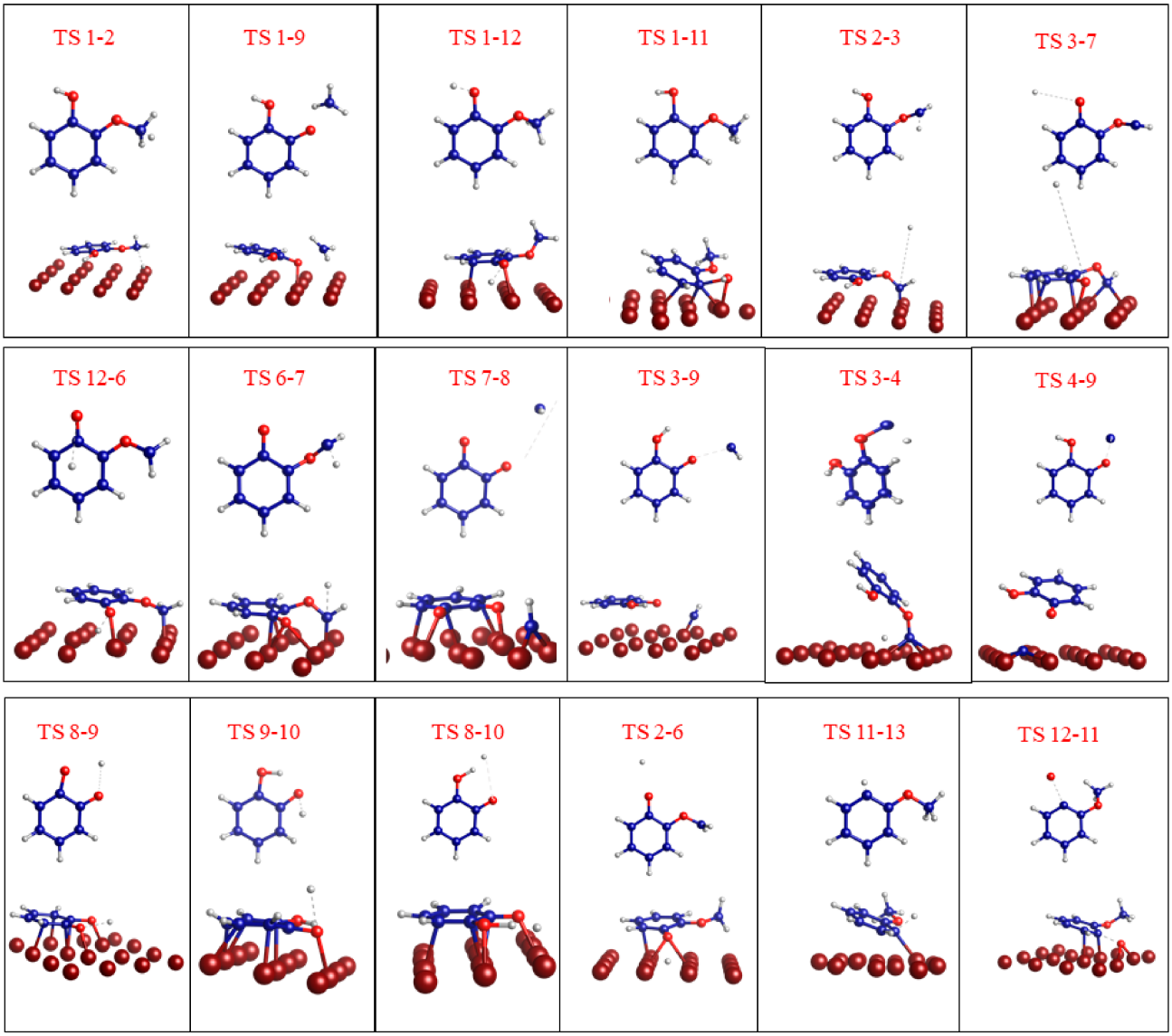

Figure 4. Top and side views of the geometries of the various transition state structures involved in the HDO reaction of guaiacol on Cu (111). Cu: brown; O: red; C: blue; H: white. The top views are transition state structures shown without the Cu (111) surface atoms. The side views are the transition state structures shown with the Cu (111) interacting surface atoms. The broken lines indicate the bonds being formed and broken.

The transition state (TS) structures identified along the different pathways 1–4 are also shown in Figure 4. Where the notations e.g., TS 1–2 are the transition state structure between the ground state structures **1** and 2, i.e., structure **1** transforming to 2. The broken lines in Figure 4, show bonds that are being broken in the activated complex, and bonds that are being formed.

3. Results and Discussion

3.1. Adsorption of Desired Compounds and Their Charge Density Difference Plots

After horizontal adsorption of the aromatic compounds on the surface, as seen from the top views in Figure 2, guaiacol and catechol prefer to adsorb on the top Cu site. Whiles anisole is displaced after optimization to the bridge Cu site on the surface. The aromatic molecules guaiacol, anisole, and catechol weakly adsorbed horizontally and parallel to the copper surface with an average bond distance of 2.6 Å between the carbons in the benzene rings and the Cu surface atoms. As shown in Table 2, the binding energies show

that catechol adsorption is the most favorable thermodynamically, and anisole adsorption is the least favored.

Table 2. Adsorption energies (eV) of guaiacol, catechol, and anisole on Cu (111) and their average bond distances (Å) from the copper surface.

Compound	E_{ads}/eV	d $_{(Cu–C)}$/Å
Guaiacol	−1.90	2.61
Catechol	−2.18	2.59
Anisole	−0.72	2.61

Further insight into the nature of the substrate-adsorbate interactions and charge redistribution between the adsorbate and the Cu (111) surface can be obtained from the iso-surfaces of the induced charge density ($\Delta\rho$) plot, which was calculated using the equation:

$$\Delta\rho = (\rho_{Cu+adsorbate}) - (\rho_{Cu} + \rho_{absorbate}) \quad (3)$$

where ($\rho_{Cu+adsorbate}$) is the product charge density for the adsorbed system, ρ_{Cu} is the reactant charge density for the isolated bare surface, and $\rho_{adsorbate}$ is the reactant charge density for the isolated adsorbate.

The analysis of the differential charge density iso-surface contours (Figure 5) plotted with an iso-value of 0.006 reveals electron density accumulation within the benzene ring and the copper surface regions. The charge loss occurs on the Cu topmost layer and is transferred to the adsorbate. We also see electron density accumulation on the adsorbate, mostly in guaiacol and catechol, which is consistent with the strong binding energies of −1.90 eV and −2.18 eV reported, respectively. However, in the case of anisole, much of the charge transfer and gain occurs within the copper slab and not at the interface of the copper and anisole. As a result, the relative lack of charge transfer between surface Cu and the anisole molecule leads to weaker binding to the surface, consistent with the low binding energy of −0.72 eV in Table 1.

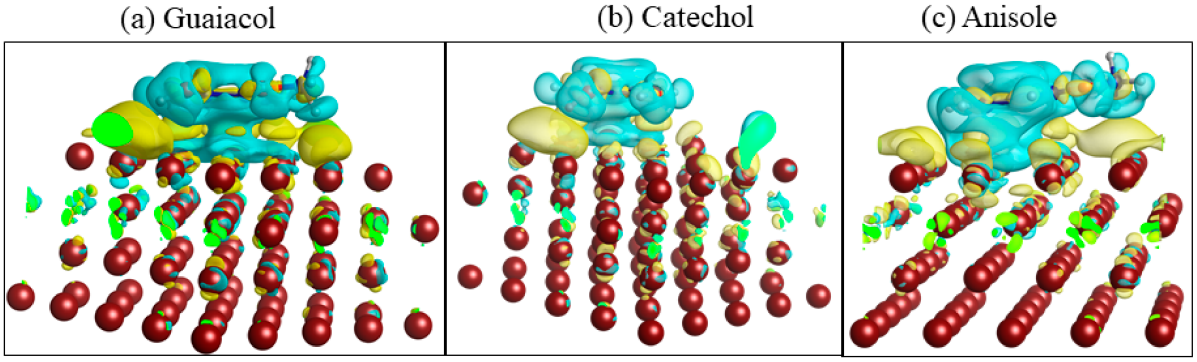

Figure 5. Charge density difference plots between the Cu (111) surface and the molecules; (**a**) guaiacol (**b**) catechol and (**c**) anisole. Colour code: yellow regions indicate electron depletion (holes) and cyan regions show electron accretion (electrons).

3.2. Mechanism of Catechol Formation

As shown in Figure 3, three pathways were considered for catechol formation. Path A involves the dehydrogenation of the methyl group of guaiacol, path B involves demethylation, and path C involves the dehydrogenation of the hydroxyl group of guaiacol. The reaction energies and activation barriers for the detailed mechanism have been computed and are shown in the reaction profile diagram (Figure 6). Guaiacol adsorbs exothermically on Cu (111) with a binding energy of −1.90 eV, see image 1 of Figure 2. Removal of hydrogen from the OH group (Path C, ΔE_a = 0.99 eV) is significantly kinetically favored

over the dehydrogenation of the methyl group (Path A, ΔE_a = 3.51 eV) and the direct demethoxylation (Path B, ΔE_a = 1.97 eV).

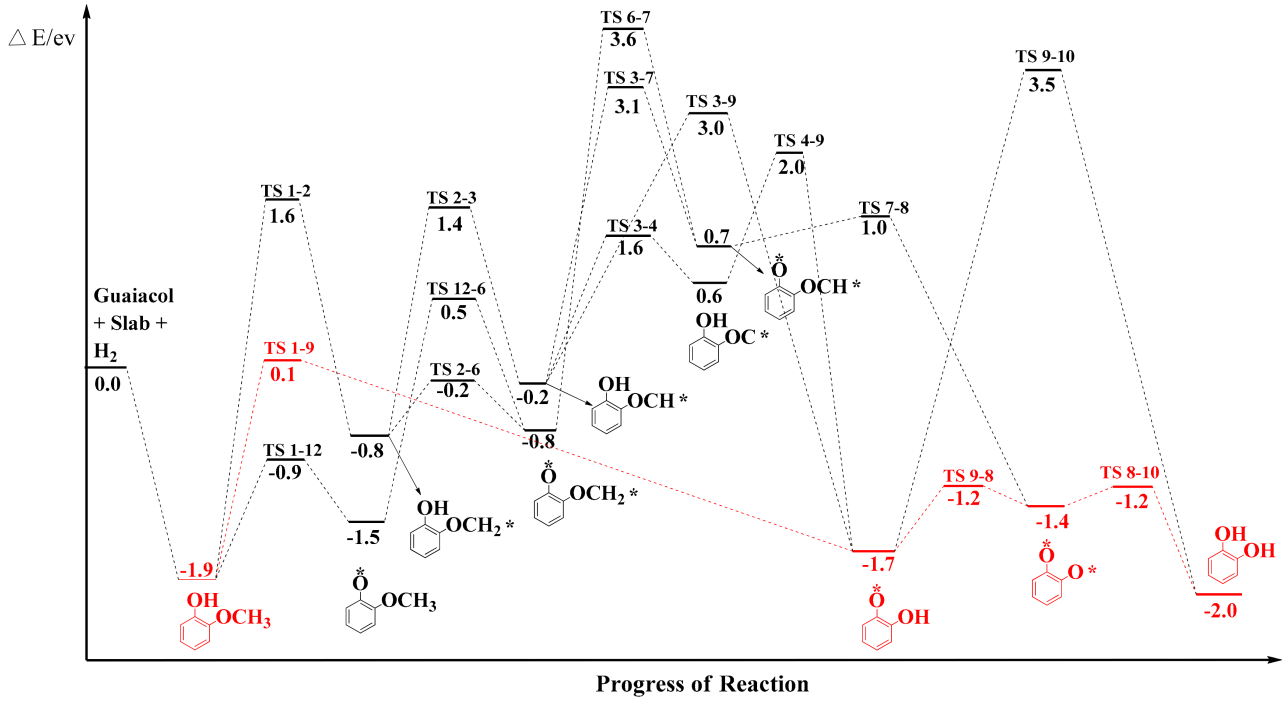

Figure 6. Energy profile diagram for catechol formation. Where the activation energies and reaction energies are reported relative to the isolated reactants i.e., guaiacol, hydrogen gas, and Cu (111) surface. The kinetically accessible pathway is highlighted in red. * indicates on the adsorbate, the sites of decomposition and radical formation.

Along path A, the dehydrogenation at the methoxy group requires a barrier of 3.51 eV to be overcome to form product **2**, which can then either be dehydrogenated via the hydroxyl or the methoxy group. The energetics show that although dehydrogenation of the hydroxyl group to form structure **6** requires a much lower energy of 0.6 eV (**TS 2–6**), the subsequent dehydrogenation step via **TS 6–7** becomes more challenging, requiring energy of 3.9 eV. These energy barriers show that the transformation of structure **2** into **3** is the preferred path. Hydrogen is further lost via **TS 2–3**, with a barrier of 2.16 eV to form product **3**. The dehydrogenation **1–2** at the methoxy group activates the C–H bonds at the aliphatic functionality in product **2**, which lowers the subsequent barriers for the dehydrogenation as seen for **TS 2–3**. Subsequently, structure **3** could either lose hydrogen from the hydroxyl or the alkoxy group. Hydrogen loss via the hydroxyl is also more challenging, requiring a transformation energy of 3.8 eV **(TS 3–7),** and further dehydrogenation into structure **5** is not possible, as structure **5** is not a stable compound on the surface. Structure **3** is more favorably converted via **TS 3–4** (E_a = 1 eV), where hydrogen is lost from the alkoxy leaving behind –OC, compared to the loss of –CH via **TS 3–9** (3.2 eV). The cleavage reaction of the C–O_{ring} bond occurs at 1.39 eV via **TS 4–9** after which structure **9** is formed. The further loss of hydroxyl hydrogen to form catecholate (structure **8**) through **TS 9–8** has a barrier of 0.5 eV. Finally, the concerted hydrogenation of structure **8** via **TS 8–10** to form catechol is favored. For the adsorbed catecholate **8**, two alternative paths have to be considered as consecutive reactions: single-step rehydrogenation **TS 8–9** at one O site or concerted rehydrogenation at both O sites **TS 8–10**. These two reactions have very low and similar energy barriers of 0.17 eV and 0.22 eV, respectively. The single-step hydrogenation step is exothermic by −1.66 eV, whereas the concerted hydrogenation step is also exothermic by −2.03 eV. A second exothermic rehydrogenation step proceeds with a much higher barrier (**TS 9–10**, ΔE_{rxn} = −2.03 eV, E_a = 5.17 eV). The initial loss of hydrogen and rehydrogenation of catecholate has been observed in previous experiments on Cu/Ni/zeolites to lead to

the formation of catechol [30]. It is seen that the single-step rehydrogenation proceeds with a lower barrier than the concerted hydrogenation, but the second rehydrogenation proceeds over a very high barrier of about 5.17 eV, indicating that catechol will be formed by concerted hydrogenation but not through stepwise hydrogenation. Along path A, guaiacol is dehydrogenated at the methoxy site sequentially to leave behind –OC. The carbon is then lost, followed by dehydrogenation of the hydroxyl to form catecholate, which again is hydrogenated concertedly into catechol. The rate-limiting step along the Path A transformation is the first dehydrogenation step of guaiacol into 2-methylene-oxy-phenol, which requiring an energy barrier of 3.51 eV to be overcome.

On pathway B, the direct $–CH_3$ removal requires a barrier of 1.97 eV to be overcome via **TS 1–9**, whereby guaiacol is transformed to hydrogen catecholate (structure **9**). Hydrogen catecholate is dehydrogenated to catecholate via a barrier of 0.5 eV through transition structure **TS 9–8**. Rehydrogenation of catecholate is concerted and leads to catechol formation as seen and discussed earlier for pathway A. The rate-determining step along this path is the direct removal of the methyl group from the methoxy through **TS 1–9**, where E_a is 1.97 eV.

Finally, on path C, the dehydrogenation of the hydroxyl group requires an energy of 1 eV through **TS 1–12**. Subsequently, the methoxy group can then be dehydrogenated in two steps. Transformations **12–6** and **6–7** occur with barriers of 2 and 3.9 eV respectively leaving –OCH behind. As discussed earlier, the direct removal of hydrogen from structure **7** to form structure **5** is not possible as structure **5** cannot be formed on the surface. Hence –CH is lost from structure **7** via **TS 7–8** which leads to the formation of the catecholate. The concerted hydrogenation of catecholate through **TS 8–9** with an energy barrier of 0.2 eV will then occur. The highest barrier along path C when forming catechol is the second dehydrogenation step of the methoxy group from structures **6** to **7** with an energy of 3.9 eV.

Comparing the rate-limiting steps which show selectively towards a given pathway, the transformation of guaiacol into catechol will occur along path B, i.e., the direct demethylation. Occurring in the following sequence: demethylation, dehydrogenation of hydroxyl, and finally concerted hydrogenation into a product, although lowering the barrier for demethylation is desirable.

3.3. Mechanism of Anisole Formation

There are two possible pathways for the formation of anisole. Pathway C entails the initial dehydrogenation of –OH of guaiacol and pathway D entails the direct dehydroxylation of –OH of guaiacol to produce anisole. Reaction energies and barriers for transformations are represented in the energy profile diagram in Figure 7.

Along path C, the removal of hydrogen from the hydroxyl group via **TS 1–12** yields guaiacolate, which occurs with an energy barrier of 0.99 eV and reaction energy of −1.50 eV. Also, $C_6H_4(O)(OCH_3)$ structure **12** undergoes further loss of oxygen **12–11** to form 2-methyl benzene-1-ide via the rate-limiting barrier of 2.7 eV. Structure **11** subsequently undergoes hydrogenation at the phenyl ring to yield anisole through the transition state, **TS 11–13** (E_a = 1.3 eV). The single-step hydrogenation, although not the highest energy barrier step, is an endothermic process (+ 0.4 eV) and a thermodynamically challenging step.

Along path D, the transformation **1–11**, i.e., the direct removal of –OH to form $C_6H_4(OCH_3)$ **11**, is kinetically demanding with an activation barrier of 2.07 eV, and this elementary step is exothermic by −0.61 eV. The hydrogenation step as seen in the previous path is less challenging with an energy barrier of 1.3 eV (**TS 11–13**), which makes the dehydroxylation step the rate-determining step along transformation path D.

Considering both reaction pathways, anisole is formed preferably by the direct removal of –OH from guaiacol followed by hydrogenation. Since the anisole formation results in a product with higher energy (less stable), anisole should be decomposed easily.

The energetically most favorable reaction path from guaiacol to catechol and anisole is summarized in Figure 8. The stepwise barriers reported in Figure 8 show that the Cu (111) surface favors catechol formation over anisole, as the rate-limiting barrier is higher by 0.1 eV

for anisole formation than for catechol production and the product formed, i.e., catechol, is thermodynamically more stable than anisole. Anisole is more likely to disintegrate back into guaiacol, implying that the formation of catechol is thermodynamically and kinetically preferred over anisole on the Cu (111) surface. The mechanism of Guaiacol conversion on Cu (111) is similar to the Pt (111) [34] surface via pathway B, whiles the Ru (0001) [15] surface prefers pathway A, i.e., the dehydrogenation of the methoxy group of guaiacol.

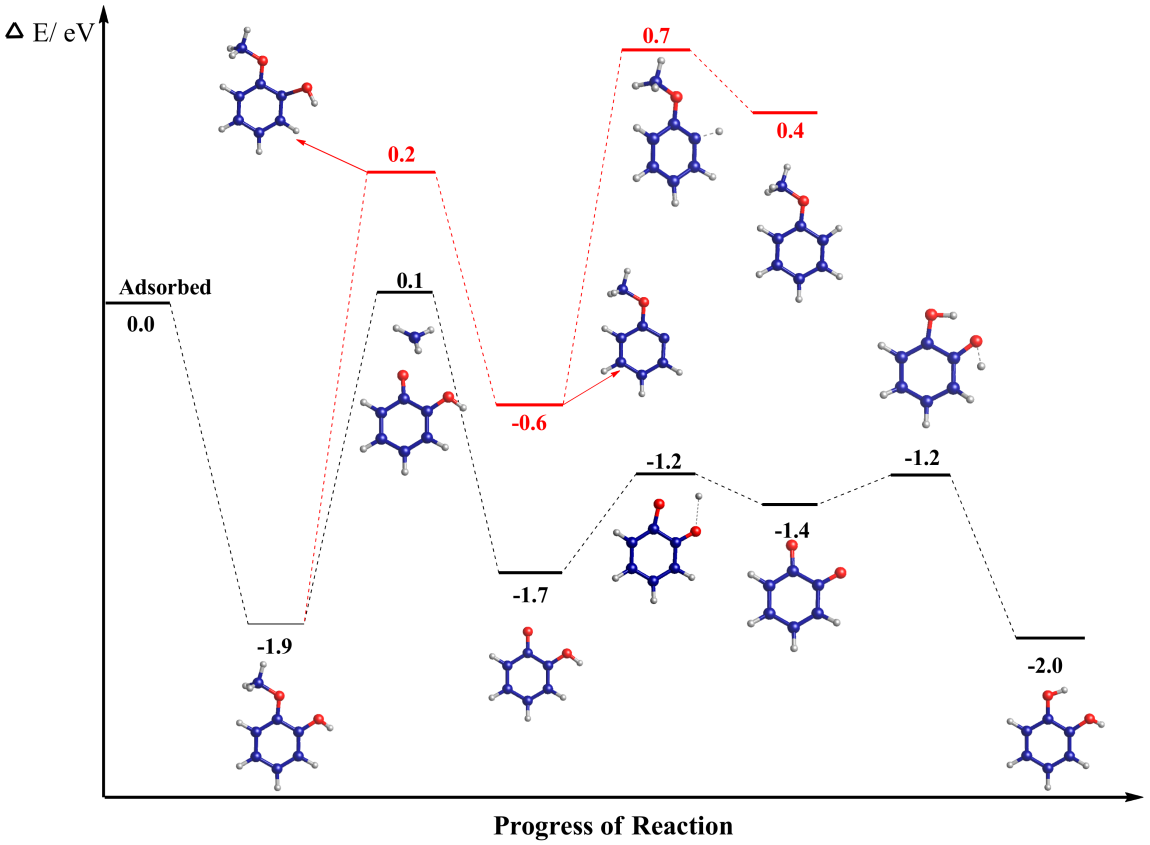

Figure 7. Energy profile diagram for anisole formation, where the activation energies and reaction energies are reported relative to the isolated reactants, i.e., guaiacol, hydrogen gas, and Cu (111) surface. The kinetically accessible pathway is highlighted in red. The broken lines indicate the bonds being formed and broken.

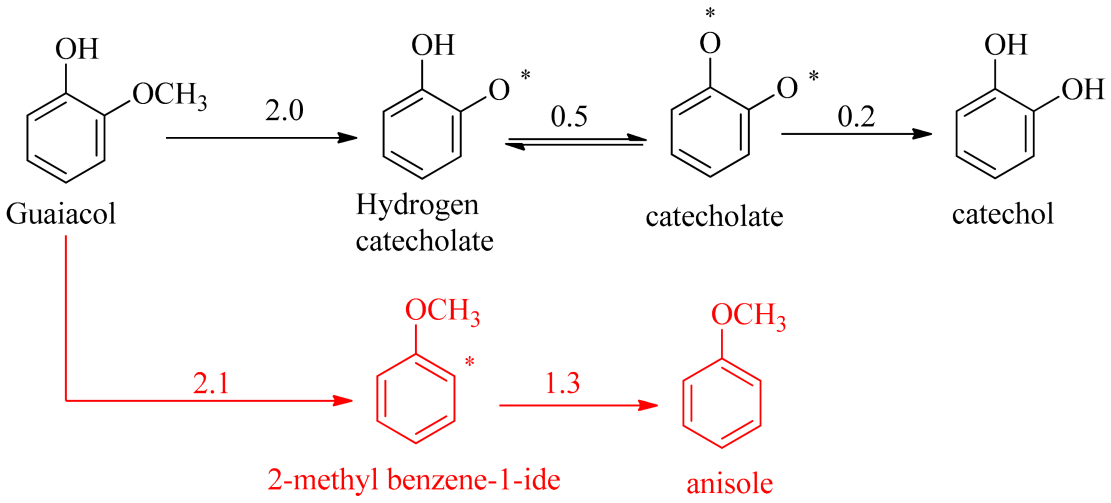

Figure 8. Overall proposed reaction steps for the conversion of guaiacol to catechol and anisole on Cu (111). Numerical values over the arrows denote activation energies for individual elementary steps in eV. * indicates on the adsorbate, the sites of decomposition and radical formation.

4. Conclusions

We have investigated the hydrodeoxygenation mechanism of guaiacol on the Cu (111) surface. Our results indicate that the transformation of guaiacol into catechol will occur via a direct demethylation pathway, in the following sequence: demethylation, dehydrogenation of hydroxyl, and finally concerted hydrogenation into a product, although it would be desirable if the barrier for demethylation could be lowered. Here, we should note, however, that the energy barriers calculated in this work could be considered as a worst-case scenario, as defects on an experimental Cu (111) surface, e.g., surface vacancies and low-coordinated edge and corner sites, would be more reactive leading to lower energy barriers.

Direct –OH (dehydroxylation) removal leads to the formation of a less stable product, i.e., anisole, whose formation is challenging compared to catechol. This comparison shows that catechol should be formed selectively on the Cu (111) surface, which will therefore be the major product of anisole. However, due to its instability, anisole could be a precursor to the formation of other interesting deoxygenated compounds.

Author Contributions: Research data collection and draft manuscript preparation, D.K., research concept development, supervision, grant acquisition and manuscript revisions, C.R.K., N.H.d.L., R.T. and E.A. All authors have read and agreed to the published version of the manuscript.

Funding: This research was funded by the Leverhulme Trust—UK Royal Society under the Royal Society Leverhulme Africa Postdoctoral Fellowships 2018. As well as the Royal Society—UK Department for International Development under the Africa Capacity Building Initiative. It was also funded by The World Academy of Sciences, under the TWAS programme basic sciences individuals 2018.

Acknowledgments: C.R.K. is grateful for funding from The World Academy of Sciences (grant 18-032 RG/CHE/AF/AC_I). C.R.K., R.T., and N.H.d.L. acknowledge the UK Royal Society and Leverhulme Trust for a research grant under the Royal Society-Leverhulme Africa Postdoctoral Fellowship Award Scheme (grant LAF\R1\180013). N.H.d.L. and E.A. acknowledge the Royal Society and UK Department for International Development for the grant under the Africa Capacity Building Initiative (Programme grant AQ140028) and for funding the APC. The authors acknowledge the Centre for High-Performance Computing (CHPC), South Africa, for additional computing resources.

Conflicts of Interest: The authors declare no conflict of interest.

References

1. Zakzeski, J.; Bruijnincx, P.C.A.; Jongerius, A.L.; Weckhuysen, B.M. The catalytic valorization of lignin for the production of renewable chemicals. *Chem. Rev.* **2010**, *110*, 3552–3599. [CrossRef] [PubMed]
2. Kunkes, E.L.; Simonetti, D.A.; West, R.M.; Serrano-Ruiz, J.C.; Gärtner, C.A.; Dumesic, J.A. Catalytic conversion of biomass to monofunctional hydrocarbons and targeted liquid-fuel classes. *Science* **2008**, *322*, 417–421. [CrossRef] [PubMed]
3. Saidi, M.; Samimi, F.; Karimipourfard, D.; Nimmanwudipong, T.; Gates, B.C.; Rahimpour, M.R. Upgrading of lignin-derived bio-oils by catalytic hydrodeoxygenation. *Energy Environ. Sci.* **2014**, *7*, 103–129. [CrossRef]
4. Xu, C.; Arancon, R.A.D.; Labidi, J.; Luque, R. Lignin depolymerisation strategies: Towards valuable chemicals and fuels. *Chem. Soc. Rev.* **2014**, *43*, 7485–7500. [CrossRef]
5. Li, C.; Zhao, X.; Wang, A.; Huber, G.W.; Zhang, T. Catalytic transformation of lignin for the production of chemicals and fuels. *Chem. Rev.* **2015**, *115*, 11559–11624. [CrossRef] [PubMed]
6. Fisk, C.A.; Morgan, T.; Ji, Y.; Crocker, M.; Crofcheck, C.; Lewis, S.A. Bio-oil upgrading over platinum catalysts using in situ generated hydrogen. *Appl. Catal. A Gen.* **2009**, *358*, 150–156. [CrossRef]
7. He, Z.; Wang, X.; Laurent, E.; Delmon, B. Hydrodeoxygenation of model compounds and catalytic systems for pyrolysis bio-oils upgrading. *Catal. Sustain. Energy* **2012**, *1*, 28–52. [CrossRef]
8. Wildschut, J.; Mahfud, F.H.; Venderbosch, R.H.; Heeres, H.J. Hydrotreatment of fast pyrolysis oil using heterogeneous noble-metal catalysts. *Ind. Eng. Chem. Res.* **2009**, *48*, 10324–10334. [CrossRef]
9. Kumaniaev, I.; Samec, J.S.M. Adsorption isotherms of lignin-derived compounds on a palladium catalyst. *Ind. Eng. Chem. Res.* **2019**, *58*. [CrossRef]
10. Paone, E.; Espro, C.; Pietropaolo, R.; Mauriello, F. Selective arene production from transfer hydrogenolysis of benzyl phenyl ether promoted by a co-precipitated Pd/Fe3O4 catalyst. *Catal. Sci. Technol.* **2016**, *6*, 7937–7941. [CrossRef]
11. Dai, G.; Zhu, Y.; Yang, J.; Pan, Y.; Wang, G.; Reubroycharoen, P.; Wang, S. Mechanism study on the pyrolysis of the typical ether linkages in biomass. *Fuel* **2019**, *249*, 146–153. [CrossRef]
12. Mäki-Arvela, P.; Murzin, D.Y. Hydrodeoxygenation of lignin-derived phenols: From fundamental studies towards industrial applications. *Catalysts* **2017**, *7*, 265. [CrossRef]

13. Luo, Z.; Wang, Y.; He, M.; Zhao, C. Precise oxygen scission of lignin derived aryl ethers to quantitatively produce aromatic hydrocarbons in water. *Green Chem.* **2015**, *18*, 433–441. [CrossRef]
14. Liu, G.; Robertson, A.W.; Li, M.M.-J.; Kuo, W.C.H.; Darby, M.T.; Muhieddine, M.H.; Lin, Y.-C.; Suenaga, K.; Stamatakis, M.; Warner, J.H.; et al. MoS2 monolayer catalyst doped with isolated Co atoms for the hydrodeoxygenation reaction. *Nat. Chem.* **2017**, *9*, 810–816. [CrossRef]
15. Chiu, C.-C.; Genest, A.; Borgna, A.; Rösch, N. Hydrodeoxygenation of guaiacol over Ru(0001): A DFT study. *ACS Catal.* **2014**, *4*, 4178–4188. [CrossRef]
16. Nimmanwudipong, T.; Aydin, C.; Lu, J.; Runnebaum, R.C.; Brodwater, K.C.; Browning, N.D.; Block, D.E.; Gates, B.C. Selective hydrodeoxygenation of guaiacol catalyzed by platinum supported on magnesium oxide. *Catal. Lett.* **2012**, *142*, 1190–1196. [CrossRef]
17. Wan, H.; Chaudhari, R.V.; Subramaniam, B. Catalytic hydroprocessing of p-cresol: Metal, solvent and mass-transfer effects. *Top. Catal.* **2012**, *55*, 129–139. [CrossRef]
18. Jin, S.; Guan, W.; Tsang, C.-W.; Yan, D.Y.S.; Chan, C.-Y.; Liang, C. Enhanced hydroconversion of lignin-derived oxygen-containing compounds over bulk nickel catalysts though Nb2o5 modification. *Catal. Lett.* **2017**, *147*, 2215–2224. [CrossRef]
19. Zhao, C.; Kou, Y.; Lemonidou, A.A.; Li, X.; Lercher, J.A. Hydrodeoxygenation of bio-derived phenols to hydrocarbons using RANEY® Ni and Nafion/SiO_2catalysts. *Chem. Commun.* **2010**, *46*, 412–414. [CrossRef]
20. Ohta, H.; Kobayashi, H.; Hara, K.; Fukuoka, A. Hydrodeoxygenation of phenols as lignin models under acid-free conditions with carbon-supported platinum catalysts. *Chem. Commun.* **2011**, *47*, 12209–12211. [CrossRef]
21. Girgis, M.J.; Gates, B.C. Reactivities, reaction networks, and kinetics in high-pressure catalytic hydroprocessing. *Ind. Eng. Chem. Res.* **1991**, *30*, 2021–2058. [CrossRef]
22. Lesnard, H.; Bocquet, M.-L.; Lorente, N. Dehydrogenation of aromatic molecules under a scanning tunneling microscope: Pathways and inelastic spectroscopy simulations. *J. Am. Chem. Soc.* **2007**, *129*, 4298–4305. [CrossRef] [PubMed]
23. Mittendorfer, F.; Hafner, J. Hydrogenation of benzene on Ni(111)A DFT study. *J. Phys. Chem. B* **2002**, *106*, 13299–13305. [CrossRef]
24. Morin, C.; Simon, D.; Sautet, P. Density-functional study of the adsorption and vibration spectra of benzene molecules on PT(111). *J. Phys. Chem. B* **2003**, *107*, 2995–3002. [CrossRef]
25. Honkela, M.L.; Björk, J.; Persson, M. Computational study of the adsorption and dissociation of phenol on Pt and Rh surfaces. *Phys. Chem. Chem. Phys.* **2012**, *14*, 5849. [CrossRef]
26. Zhang, F.; Johnson, D.M.; Wang, J.; Liu, S.; Zhang, S. Measuring the regional availability of forest biomass for biofuels and the potential of GHG reduction. *Energies* **2018**, *11*, 198. [CrossRef]
27. Site, L.D.; Alavi, A.; Abrams, C.F. Adsorption energies and geometries of phenol on the (111) surface of nickel: Anab initiostudy. *Phys. Rev. B* **2003**, *67*, 1–3. [CrossRef]
28. Bonalumi, N.; Vargas, A.; Ferri, D.; Baiker, A. Catalytic chiral metal surfaces generated by adsorption ofO-phenyl derivatives of cinchonidine. *J. Phys. Chem. C* **2007**, *111*, 9349–9358. [CrossRef]
29. Yang, J.; Williams, C.L.; Ramasubramaniam, A.; Dauenhauer, P.J. Aqueous-phase hydrodeoxygenation of highly oxygenated aromatics on platinum. *Green Chem.* **2014**, *16*, 675–682. [CrossRef]
30. Kumar, R.; Strezov, V.; Lovell, E.; Kan, T.; Weldekidan, H.; He, J.; Dastjerdi, B.; Scott, J. Bio-oil upgrading with catalytic pyrolysis of biomass using Copper/zeolite-Nickel/zeolite and Copper-Nickel/zeolite catalysts. *Bioresour. Technol.* **2019**, *279*, 404–409. [CrossRef]
31. Ben, H.; Ferguson, G.A.; Mu, W.; Pu, Y.; Huang, F.; Jarvis, M.; Biddy, M.; Deng, Y.; Ragauskas, A.J. Hydrodeoxygenation by deuterium gas–A powerful way to provide insight into the reaction mechanisms. *Phys. Chem. Chem. Phys.* **2013**, *15*, 19138–19142. [CrossRef]
32. Jenkins, S.J. Aromatic adsorption on metals via first-principles density functional theory. *Proc. R. Soc. A Math. Phys. Eng. Sci.* **2009**, *465*, 2949–2976. [CrossRef]
33. Badawi, M.; Paul, J.-F.; Payen, E.; Romero, Y.; Richard, F.; Brunet, S.; Popov, A.; Kondratieva, E.; Gilson, J.-P.; Mariey, L.; et al. Hydrodeoxygenation of phenolic compounds by sulfided (Co) Mo/Al2O3 catalysts, a combined experimental and theoretical study. *Oil Gas Sci. Technol. Rev. de l'IFP* **2013**, *68*, 829–840. [CrossRef]
34. Lee, K.; Gu, G.H.; Mullen, C.A.; Boateng, A.A.; Vlachos, D.G. Guaiacol hydrodeoxygenation mechanism on PT(111): Insights from density functional theory and linear free energy relations. *ChemSusChem* **2014**, *8*, 315–322. [CrossRef] [PubMed]
35. Kohn, W.; Sham, L.J. Self-consistent equations including exchange and correlation effects. *Phys. Rev.* **1965**, *140*, A1133–A1138. [CrossRef]
36. Perdew, J.P.; Burke, K.; Ernzerhof, M. Generalized gradient approximation made simple. *Phys. Rev. Lett.* **1996**, *77*, 3865. [CrossRef]
37. Giannozzi, P.; Baroni, S.; Bonini, N.; Calandra, M.; Car, R.; Cavazzoni, C.; Ceresoli, D.; Chiarotti, G.L.; Cococcioni, M.; Dabo, I.; et al. QUANTUM ESPRESSO: A modular and open-source software project for quantum simulations of materials. *J. Phys. Condens. Matter* **2009**, *21*, 395502. [CrossRef]
38. Greeley, J.P.; Nørskov, J.K.; Mavrikakis, M. Electronicstructure andcatalysis onmetalsurfaces. *Annu. Rev. Phys. Chem.* **2002**, *53*, 319–348. [CrossRef]
39. Pack, J.D.; Monkhorst, H.J. "Special points for Brillouin-zone integrations"—A reply. *Phys. Rev. B* **1977**, *16*, 1748–1749. [CrossRef]
40. Runnebaum, R.C.; Nimmanwudipong, T.; Block, D.E.; Gates, B.C. Catalytic conversion of compounds representative of lignin-derived bio-oils: A reaction network for guaiacol, anisole, 4-methylanisole, and cyclohexanone conversion catalysed by Pt/γ-Al2O3. *Catal. Sci. Technol.* **2012**, *2*, 113–118. [CrossRef]